ACES Asian Chemical Editorial Society

DOI: 10.1002/asia.201500974

CHEMISTRY AN ASIAN JOURNAL Full Paper

Surface Chemistry

A Versatile Anisometric Metallic Supercrystal with Controllable Orientation on a Chip as a Stable and Reliable Label-Free Biosensor

Li Qiu,[a] Wei Qiang Wang,[b] Nan Nan Zhang,[b] Hao Wei Jia,[a] Jin Wang,*[a] and Hong Hua Ge[b]

Abstract: Based on anisometric noble-metal nanocrystals, a universal fabrication protocol for preparing 3D supercrystals with controlled orientation on a chip has been developed. A comparison of the surface-enhanced Raman scattering (SERS) behavior of 3D nanorod supercrystals aligned vertically and parallel to the chip indicates that the SERS-enhancing ability and reproducibility of the former is superior to the latter. The 3D nanorod supercrystals aligned vertically to the chip have been utilized as highly sensitive SERS substrates for the label-free discrimination of Gram-positive and -negative bacteria. Furthermore, to strengthen the stability of the supercrystal substrate for assays of bacteria in biosamples, a coating of the antibiotic vancomycin can dramatically increase adhesion of bacteria on a nanointerface and simultaneously improve the SERS response of bacteria to achieve a layer-by-layer assembled, stable, and reliable biosensor for bacteria.

Introduction

Recently, noble metallic nanoparticles have been assembled to form plasmonic superstructures, which have extensive applications in surface-enhanced Raman scattering (SERS),[1–3] biological delivery,[4] plasmonic ruler,[5,6] catalytic,[7] photothermal therapy,[8] and so forth, owing to the collective oscillation of free electrons in the superstructure. It is known that plasmonic sensing of noble metallic nanoparticles is highly dependent on the shape or size of the plasmonic nanostructure. Therefore, the assembly of anisometric nanoparticles to yield superstructures has been attracting more attention. Different strategies and technologies, for example, gravity-driven self-assembly,[9] biotemplates,[10] supramolecular templates,[11] inorganic species,[12] and evaporation,[13,14] have been employed to fabricate anisometric superstructures.

Controlling the orientation of an anisometric assembly on a chip is difficult and challenging. Recently, evaporation-induced self-assembly of cetyl trimethylammonium bromide (CTAB)-coated gold nanorods (AuNRs) has led to the formation of highly organized vertical monolayer arrays on arbitrary substrates.[15] In addition, based on the hydrophobicity of a substrate, the selective arrangement of assembled AuNRs on unstructured substrates can be realized by using a removable elastomer grafting stamp.[16] Experimental results suggest that the direction of the assembly of the AuNRs is parallel to the grating on a silicon substrate; however, the direction of assembly of the AuNRs is perpendicular to the grating on indium tin oxide (ITO) substrate. Different from previous reports, we propose a universal protocol, that is, controllable chemical functionalization combined with controllable physical evaporation to yield anisometric metallic supercrystals with controllable orientation, including that vertical or parallel to the chip.

Recently, 3D AuNR supercrystals have been introduced as a surface-enhanced Raman scattering (SERS) substrate for the detection of scrambled prions or food contaminants such as melamine.[15,17] However, current SERS assays of pathogenic bacteria are mainly limited to single plasmonic nanoparticles or unordered aggregates of gold or silver nanoparticles.[18–20] Liu et al. successfully utilized anodic aluminum oxide (AAO) as a template to fabricate silver nanoparticle arrays with sub-10 nm interparticle gaps and employed the highly uniform AAO-SERS substrate to achieve SERS sensing of the bacteria *Escherichia coli* and *Lactobacillus plantarum*.[21] Herein, based on an as-fabricated anisometric metallic supercrystal substrate with controllable orientation on a chip, we developed a novel, stable SERS biosensor with large-scale uniformity and ultrasensitivity for sensing Gram-positive and -negative bacteria.

[a] *L. Qiu,[+] H. W. Jia, Prof. Dr. J. Wang*
Institute of Intelligent Machines, Chinese Academy of Sciences
Hefei, Anhui 230031 (P.R. China)
E-mail: jwang@iim.ac.cn

[b] *W. Q. Wang,[+] Dr. N. N. Zhang, Prof. Dr. H. H. Ge*
Institute of Health Science and School of Life Science
AnHui University, Hefei, Anhui
230601 (P.R. China)

[+] *These authors contributed equally to this work.*

Supporting information for this article is available on the WWW under http://dx.doi.org/10.1002/asia.201500974.

Results and Discussion

Formation of 3D Anisometric Supercrystals with Controllable Orientations on a Chip

Effect of the Concentration of Nanoparticles on 3D Anisometric Supercrystals with Controllable Orientations on a Chip

Typical anisometric nanocrystals, including nanorods or nanoprisms, can be considered as building blocks of supercrystals owing to their unique anisotropic characteristics, such as orientation-dependent optical responses. Representative AuNRs with an aspect ratio of about 3 can be detected in the UV/Vis/near-infrared (NIR) spectrum (Figure 1 A) by a transverse plasmonic band at $\lambda = 511$ nm and a longitudinal plasmonic band at $\lambda = 678$ nm. For gold nanoprisms (AuNPs) with an aspect ratio of about 20, the UV/Vis/NIR spectrum (Figure 2 A) reveals an in-plane dipole resonance at $\lambda = 926$ nm and an in-plane quadrupole resonance at $\lambda = 627$ nm. Additionally, no plasmonic band at $\lambda = 523$ nm, corresponding to gold nanospheres (AuNSs), can be observed, which suggests that the high purity of AuNPs or AuNRs is appropriate for the fabrication of anisometric supercrystals. As far as the effects of assembling anisometric nanoparticles are concerned, the concentration of nanoparticles, surfactant, components of the metallic nanoparticles, morphology of the nanoparticles, and so forth can affect the formation of supercrystals with controllable orientations on a chip.

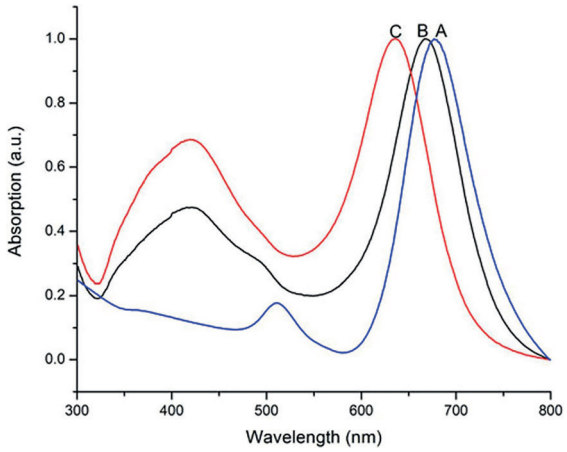

Figure 1. Normalized UV/Vis/NIR spectra of A) AuNRs, B) Au@AgNRs with a thin Ag shell of about 3 nm, and C) Au@AgNRs with a thick Ag shell of about 10 nm.

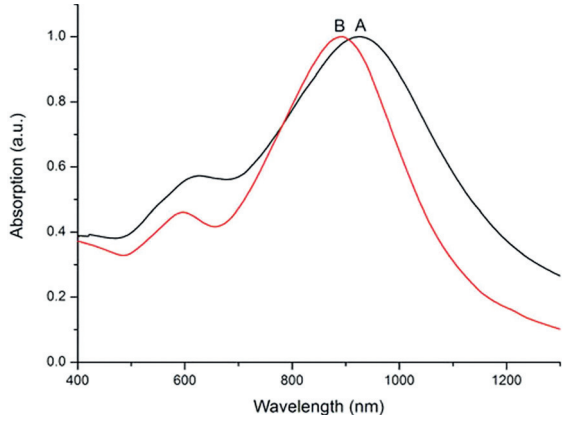

Figure 2. Normalized UV/Vis/NIR spectra of A) triangular AuNPs and B) truncated triangular AuNPs.

First, the concentration of the nanoparticles is the most important factor in controlling the orientation of an anisometric assembly on a chip. If the concentration of the nanoparticles (e.g., nanorods) is less than 0.1 nM, an axial alignment of nanorods assembles on a chip in a parallel pattern to form tape-like nematic supercrystals (as shown in Figure S1 in the Supporting Information). If the concentration of nanoparticles (e.g., nanorods) is between 1 and 20 nM, an axial alignment of nanorods assembles on a chip in a parallel pattern (as observed in Figure S2 in the Supporting Information). If the concentration of nanoparticles (e.g., nanorods) is above 50 nM, an axial alignment of nanorods assembles on a chip in a vertical pattern to yield a columnar assembly (as observed in Figure S3 in the Supporting Information). Hence, an increased density of nanorods on a chip can be favorable for the formation of a vertical array because during deposition the incoming nanorods can be efficiently supported by adjacent nanorods. However, a pure array vertical or parallel to the chip cannot be obtained only through tuning the concentration of nanoparticles.

Effect of Surfactants on Orientation-Controllable Anisometric Supercrystals on a Chip

The orientation of supercrystals on a chip is related to the amount and type of surfactant. In the case of anisometric nanoparticles, they tend to form a uniform distribution on a chip as a result of much stronger interparticle attraction between anisometric particles, in contrast with isometric nanoparticles.[22] However, if nanoparticles are coated with surfactant or dispersed in surfactant dielectric environments, interfacial deformation between the nanoparticles and chip is dramatically energetically unfavorable, which inhibits interfacial deformation and simultaneously restores the coffee-ring effect through decreasing the tension of the liquid drop. Although electrostatic repulsion between positively charged CTAB surfactant molecules is unfavorable and causes stacking of the AuNRs, another important effect, namely, attractive depletion among micelle molecules with CTAB as the depleter, can effectively drive the entropic stacking of AuNRs. Changes to the CTAB density on the AuNRs have been achieved through repeated centrifugation and rinsing steps, and the results (Figure S4 in the Supporting Information) indicate that removal of the surfactant can destroy the ordered assembly of nanorods on a chip, which leads to unordered aggregation on the substrate. On the other hand, if we redisperse AuNRs into a 0.01 M solution of CTAB surfactant, mediation by CTAB can drive the nanorods together again to recover the formation of the 3D supercrystal (observed from Figure S5 in the Supporting Infor-

mation). Hence, a balance of depletion interactions and electrostatic repulsion can contribute to the stacking of nanorods.

To explore the type of surfactant suitable for use in the assembly of nanoparticles, thiolated molecules, for example, SH-PEG or SH-PEG-NH_2 (PEG = polyethylene glycol), have been selected to replace CTAB. Herein, the thiolated polymer can be considered as a chemical anchoring agent owing to strong interactions between the thiol group and metallic surface to introduce covalent interactions into the assembly process. The radius of the ends of the nanorods can clearly affect the extent of binding between CTAB and the surface of the nanorods. The relatively loose coating of CTAB at the ends of the nanorods compared with that on the sides can cause preferential removal of the CTAB bilayer from the ends of the nanorods. If CTAB-coated nanorods are replaced with SH-PEG, the replacement process can be initiated from the ends of the nanorods, followed by the sides. On the basis of SH-PEG end-capped nanorods (2 $\mu g\,mL^{-1}$, 50 μL) with concentration of 5 nM, interactions between CTAB as a binding agent distributed along the edges of the nanorods can lead to side-by-side assembly of a 3D supercrystal parallel to the chip through electrostatic repulsion and attraction forces (Figure 3). Increasing the final

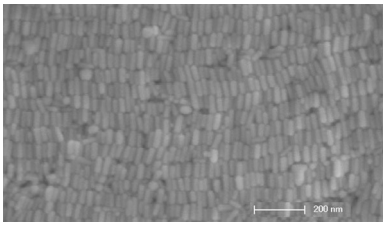

Figure 3. SEM image of pure 3D nanorod supercrystals parallel to the chip.

amount of SH-PEG added to beyond 10 $\mu g\,mL^{-1}$ (100 μL) covers all facets of the nanorods, which means the 3D supercrystal parallel to the chip can be distorted to form unordered aggregates (Figure S6 in the Supporting Information). We utilized a synergistic protocol of facet-blocking technology and tuning of the colloidal concentration to obtain 3D supercrystals parallel to the chip.

To obtain axial alignment of nanorods vertical to the chip, we adopted an analogous strategy to fabricate end-to-end assembled 3D supercrystals vertical to the chip by using another chemical blocking agent, namely, SH-PEG-NH_2. If the amount of 2 $\mu g\,mL^{-1}$ SH-PEG-NH_2 added is less than 50 μL to coat the ends of the nanorods, the interactions between ends of the nanorods can be efficiently strengthened owing to Au–N interactions. Additionally, dipole interactions between the amine groups of SH-PEG-NH_2 and the hydroxyl groups of the chip can be dramatically enhanced, which leads to binding between the ends of the nanorods and the chip. Hence, SH-PEG-NH_2 end-capped nanorods (2 $\mu g\,mL^{-1}$, 50 μL) with a concentration of 50 nM can easily yield 3D supercrystals vertical to the chip (Figure 4). Increasing the amount of SH-PEG-NH_2 added to beyond 10 $\mu g\,mL^{-1}$ (100 μL) to cover all nanorod facets, the 3D supercrystal vertical to the chip can be distorted to form unor-

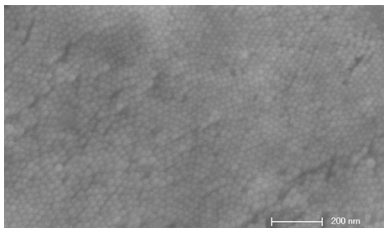

Figure 4. SEM image of pure 3D nanorod supercrystals vertical to the chip.

dered aggregates (Figure S7 in the Supporting Information). Therefore, a technique to aid facet anchoring can be introduced into the fabrication of oriented nanoarrays on a substrate.

To explore the universality of the present protocol, another anisometric nanoparticle, for example, triangular nanoprisms, can be used for orientation-controllable assembly. Similar to nanorods, with a high concentration of nanoprisms, that is, a high density of nanoprisms distributed on the substrate, the nanoprisms tend to arrange vertically to the chip. In contrast, a low concentration of nanoprisms can lead to the formation of a columnar array parallel to the chip. Similarly, if functionalization of the thiolated molecules has been introduced into the nanoprisms, functionalization could be initiated from the edges of the nanoprism, followed by the top triangular face of the nanoprism. The top triangular face of the nanoprisms is {111},[23] and the side facets are high-energy {110}, {111} or {100} facets;[24,25] this leads to greater ligand exchange at the side facets compared with that at the top triangular faces. According to the ligand absorption model proposed by Murray et al., thiolated ligand exchange on gold nanoparticles can be quickly carried out at crystal defect sites, for example, at higher energy side or apex crystal facets of the nanoprism.[26] Hence, selective functionalization of thiolated molecules on different facets of AuNPs can effectively improve the purity of supercrystal orientation on the substrate. As shown in Figure 5, if the AuNP is coated with SH-PEG, 3D lamellar supercrystals parallel to the chip can be obtained. To confirm the formation of 3D lamellar supercrystals parallel to the chip, AFM was performed to investigate the layers of the supercrystal. As shown in Figure S8 in the Supporting Information, the vertical height of the 3D lamellar supercrystal parallel to the chip is 77.8 nm.

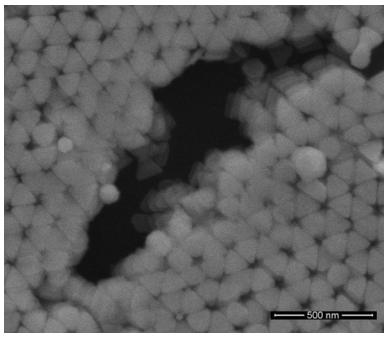

Figure 5. SEM image of 3D nanoprism supercrystals parallel to the chip.

According to a previous report on AuNPs, the thickness is usually about 5–10 nm;[27] moreover, the number of layers of 3D lamellar supercrystals parallel to the chip is approximately 8–16 layers, as confirmed by SEM observations. Analogously, if the AuNP is functionalized with SH-PEG-NH_2, an edge-to-edge assembly vertical to the chip can be formed (Figure 6).

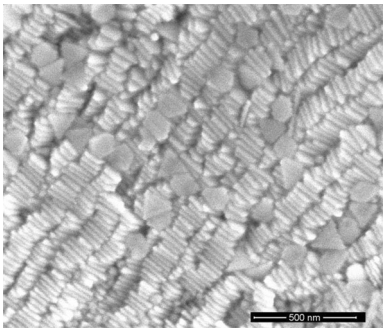

Figure 6. SEM image of 3D nanoprism supercrystals vertical to the chip.

Effects of Metallic Components and Morphologies on Orientation-Controllable Anisometric Supercrystals on a Chip

To investigate effect of the metallic component on assembly orientation on a substrate, we synthesized two different Au@AgNRs with different thicknesses of silver shell, corresponding to different silver components, namely, thicknesses of about 3–5 and 10–15 nm, as observed by TEM (Figure S9 in the Supporting Information). As shown in Figure 1 B and C, the longitudinal plasmonic bands of core–shell nanorods are blueshifted towards $\tilde{\nu}=667$ and 636 cm^{-1}, respectively, relative to those of AuNRs. As far as AuNRs are concerned, as shown in Figure 7 A, the 3D supercrystals standing on a chip can be highly ordered assemblies with a leaning pattern. In the case of the Au@AgNRs, the 3D supercrystals standing on a chip can change from a leaning pattern to a quasi-vertical pattern (Figure 7 B). Furthermore, if the AuNRs are completely coated by a thick silver shell, the 3D supercrystals standing on a chip can be assembled into a completely vertical pattern, as observed by small dots in the SEM images (e.g., see Figure 7 C). As shown in magnified SEM images (Figure S10 in the Supporting Information), the dots can actually be end caps of Au@Ag core–shell nanorods instead of nanospheres.

In addition to the effect of the metallic components, the morphology of anisometric nanoparticles is another key factor for orientation-controllable assembly on a substrate. In the case of triangular AuNPs, the sharpness of the nanoprismatic apex can clearly affect the orientation of the assembly. Herein, we synthesized truncated AuNPs to study the tips effect. As observed in Figure S11 in the Supporting Information, the tips of the AuNPs have been truncated to form nanodisks. Additionally, as shown in Figure 2, the dipole plasmonic band is blueshifted from $\lambda=924$ to 890 nm when the tips of the nanoprism are truncated; this is in agreement with previous reports.[28,29] As observed in Figure S12 in the Supporting Information, the partially ordered edge-to-edge stacking of nanoprisms vertical to the chip can be observed; however, the large-scale orientation is unordered. In the case of AuNRs, other similar rodlike nanoparticles, namely, nanorice grains with sharp ends, have been selected for assembly. As observed in Figure S13 in the Supporting Information, the ends of the nanorice grains almost are eclipsed to form the 3D nanoassembly parallel to the chip, which implies that nanorice grains tends to form end-to-end chains first, and further form eclipsed conformations of the nanorice grains parallel to the chip. In contrast, the nanorods could form side-by-side chains first, and subsequently form a sheet-to-sheet staggered arrangement parallel to the chip. It is reasonable to believe that alteration of the tips with AuNPs or AuNRs should be responsible for orientation of 3D anisometric supercrystal assemblies on a chip.

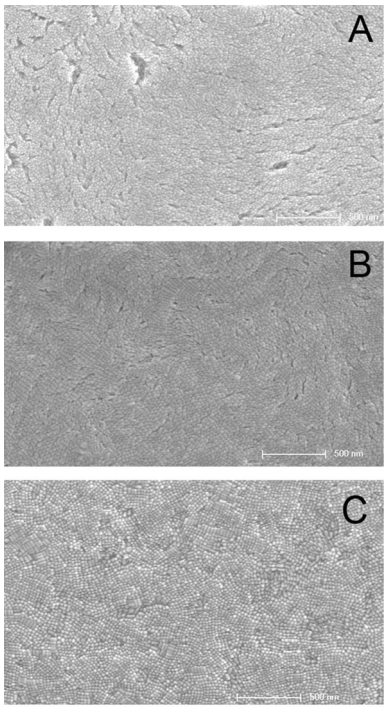

Figure 7. SEM image to show the effect of components of the Ag shell on AuNRs for 3D supercrystals vertical to the chip: A) AuNRs, B) Au@AgNRs with a thin Ag shell, and C) Au@AgNRs with a thick Ag shell.

3D Bimetallic Nanorod Supercrystals on a Chip for SERS Recognition of Bacteria

As mentioned above, two kinds of 3D anisotropic supercrystal substrates, namely, those oriented vertically and parallel to the chip, can be effectively fabricated. Herein, on the basis of AuAg bimetallic core–shell nanorod 3D supercrystals, the SERS behavior of those aligned vertically and parallel to the chip have been investigated by using the Raman probe 5,5′-dithiobis(2-nitrobezonic acid) (DTNB). Vibrations of DTNB can be efficiently enhanced with the aid of the 3D supercrystal substrate, so that excellent SERS spectra of DTNB can be recorded. The strong Raman-active band at $\tilde{\nu}=1333$ cm^{-1} can be ascribed to the symmetric stretching vibrations of the nitro group. Typical

Raman-active bands, located at $\tilde{\nu}=1066$ and 1558 cm^{-1}, respectively, can be assigned to C–N stretching and aromatic ring vibration, respectively (Figure S14 in the Supporting Information). According to point-to-point analysis of the SERS intensity of the two substrates shown in Figure S15 A and B in the Supporting Information, the coefficient of variations with 3D nanorod supercrystals aligned vertically and parallel to the chip are 4.08 and 6.13%, respectively, which suggests that the reproducibility of 3D nanorod supercrystals vertical to the chip is better than that of 3D nanorod supercrystals parallel to the chip. On the other hand, enhanced analytical factors for the 3D nanorod supercrystals vertical and parallel to the chip are 7.61×10^9 and 2.8×10^9, respectively, which indicates that the enhancement ability of 3D nanorod supercrystals vertical to the chip is superior to that of 3D nanorod supercrystals parallel to the chip. In the case of the nanoprisms, according to point-to-point analysis of the SERS intensity of 3D nanoprism supercrystals parallel and vertical to the chip (Figure S15 C and D in the Supporting Information), the coefficient variations are 4.97 and 7.54%, respectively, which indicates that the reproducibility of 3D nanoprism supercrystals parallel to the chip is clearly superior to that of nanoprism supercrystals vertical to the chip. This may be related to the uniformity of the former being better than that of the latter, as confirmed by SEM observations (Figures 5 and 6). As far as the enhanced analytical factors of 3D nanoprism supercrystals parallel and vertical to the chip are concerned, the values are 3.84×10^9 and 6.92×10^9, respectively. Based on a combination of reproducibility and enhancement factor, the 3D nanorod supercrystals vertical to the chip can be expected to act as an excellent enhanced substrate for effectively amplifying the weak inherent Raman signal of bacteria to discriminate Gram-positive and -negative bacteria.

To explore an assay with bacteria and the 3D nanorod supercrystal substrate oriented vertically to the chip, we deposited two different bacteria, namely, Gram-negative bacteria salmonella and Gram-positive bacteria staphylococcus, on the substrate. It is known that the SERS spectrum of bacteria originates from the external structure of the bacterial cell.[30] The cell wall components of Gram-positive bacteria are thick with a dense layer of peptidoglycan or teichoic acid; however, the outer membrane of the Gram-negative bacterial outer cell wall is composed of lipopolysaccharide and protein. Owing to differences between the wall structures of Gram-positive and -negative bacteria, it is reasonable to believe that the SERS spectra of salmonella and staphylococcus will be different.

First, it should be noted that the enhancement of the Raman signal of salmonella on the supercrystal substrate aligned vertically to the chip is stronger than that of the supercrystal oriented parallel to the chip. As shown in Figure 8, salmonella can adhere to the 3D supercrystal vertically aligned on a chip; this can be attributable to hydrogen bonding between the peptidoglycan of the cell and CTAB-coated supercrystal substrate. Moreover, adhesion of salmonella on the substrate of the 3D supercrystal parallel to the chip partially changes the supercrystal, which causes a decrease in the highly ordered array. In contrast, a destructive effect cannot be

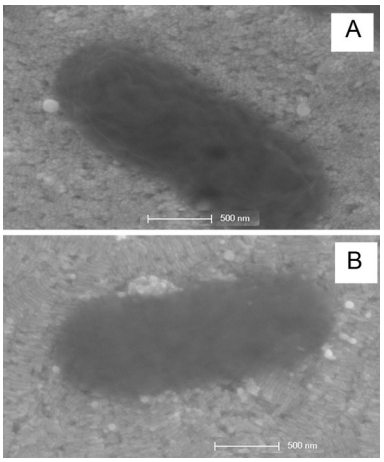

Figure 8. A) SEM image of salmonella on a substrate of bimetallic core–shell nanorod supercrystals aligned vertically to the chip. B) SEM image of salmonella on a substrate of bimetallic core–shell nanorods oriented parallel to the chip.

observed on the vertically aligned substrate; this may be ascribed to the array aligned vertically to the chip minimizing surface energy to enhance its stability relative to the loose array parallel to the chip. On the other hand, the inherent nanoantenna effect from the end-to-end assembly pattern is stronger than that of the side-by-side assembly pattern.[31] Therefore, the substrate of the 3D supercrystal vertical to the chip is almost undisturbed by attachment of the bacteria, compared with that of the 3D supercrystal substrate aligned parallel to the chip, which implies that the robustness of the former is better than that of the latter. Thus, the 3D supercrystal aligned vertically to the chip should be utilized as the SERS substrate for the sensing of different bacteria.

Representative vibrational bands of Gram-positive and -negative bacteria in SERS spectra are assigned in Tables S1 and S2 in the Supporting Information. The vibrational bands located between $\tilde{\nu}=900$ and 600 cm^{-1} can act as a fingerprint region in the spectra of bacteria. As shown in Figure 9, the strong SERS band of salmonella, which is located at $\tilde{\nu}=723$ cm^{-1}, can be attributable to ring breathing of the nucleic acid base adenosine. However, adenosine in staphylococcus is shifted towards $\tilde{\nu}=742$ cm^{-1} and split into two bands at $\tilde{\nu}=732$ and 753 cm^{-1}. The weak vibrational band at $\tilde{\nu}=792$ cm^{-1} can be assigned to ring breathing vibrations of cytosine and uracil from the nucleic acid. In the case of salmonella, the strong vibrational band at $\tilde{\nu}=663$ cm^{-1}, can be assigned to guanine; in contrast, in the case of staphylococcus, the same vibration is dramatically weaker than that of salmonella. The S–S stretching vibrations of proteins of staphylococcus and salmonella can be observed at $\tilde{\nu}=533$ cm^{-1}. The weak vibrational bands at $\tilde{\nu}=620$ and 622 cm^{-1} of salmonella and staphylococcus, respectively, can be assigned to phenylalanine skeletal vibrations of the amino acid side chain of the protein.

The Raman-active band located at $\tilde{\nu}=850$–940 cm^{-1} could be related to C–O stretching, C–O–H bending, and C–O–C bending deformation vibrations from the lipid layer components of the cell wall and membrane of salmonella; however,

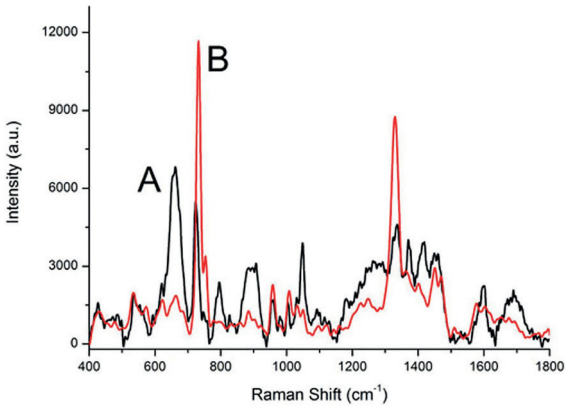

Figure 9. A) SERS spectrum of Gram-negative bacteria salmonella adhere to substrate of vancomycin coated 3D supercrystal vertical to chip. B) SERS spectrum of Gram-positive bacteria staphylococcus adhere to substrate of vancomycin coated 3D supercrystal vertical to chip.

a similar band with a different envelop at $\tilde{\nu}=870$–$940\ cm^{-1}$ could be assigned to C–O stretching, C–O–H bending, and C–O–C bending vibrations from the teichuronic acids or neutral polysaccharides of staphylococcus. The band at $\tilde{\nu}\approx1002\ cm^{-1}$ can be ascribed to vibrations of phenylalanine of both salmonella and staphylococcus. As far as both salmonella and staphylococcus are concerned, the vibrational band at $\tilde{\nu}\approx1048\ cm^{-1}$ can be assigned to the C–N and C–C stretches of carbohydrates and lipids of the cell wall.

As shown in Figure 9B, the intense vibrational band of staphylococcus at $\tilde{\nu}\approx1328\ cm^{-1}$ can be attributed to ring stretches of cytosine and uracil of DNA/RNA of the nucleic acids in Gram-positive bacteria; in contrast, the analogous vibrational band of salmonella can be observed at $\tilde{\nu}\approx1332\ cm^{-1}$.

In addition, C–H deformation vibrations, which arise from lipids, carbohydrates, and proteins of salmonella, can be observed at $\tilde{\nu}=1451\ cm^{-1}$ in the SERS spectrum. Compared with Gram-negative bacteria, C–H deformation vibrations, which originate from carbohydrates and proteins, appear at $\tilde{\nu}=1459\ cm^{-1}$ in the SERS spectrum of staphylococcus.

The vibrational band at $\tilde{\nu}=1414\ cm^{-1}$ of salmonella can be assigned to C=O symmetrical stretches of the COO^- group and originates from peptidoglycans and disaccharide–pentapeptides of the cell wall and lipopolysaccharides of the outer membrane. For Gram-positive staphylococcus, the vibrational bands at $\tilde{\nu}=1398\ cm^{-1}$ can be attributed to C=O symmetrical stretches of the COO group of carbohydrates from teichuronic acids or neutral polysaccharides.

For the C=O amide I vibration of the secondary structure of proteins of Gram-negative salmonella, the amide I skeleton of the protein can be observed at $\tilde{\nu}\approx1691\ cm^{-1}$ as a broad vibrational band. In the case of Gram-positive staphylococcus, the carboxylic stretching vibrational band of the amide I skeleton of proteins is blueshifted towards $\tilde{\nu}=1657\ cm^{-1}$ and the profile is broad compared with that of salmonella. For the N–H or C–N stretches of the amide II vibration of proteins of both salmonella and staphylococcus between $\tilde{\nu}=1550$ and $1520\ cm^{-1}$, these are absent in SERS spectra. However, in the case of the amide III vibration of the secondary structure of proteins of salmonella, the symmetric C–N stretches, N–H symmetric deformation, and C=O symmetric stretches appear between $\tilde{\nu}=1307$ and $1241\ cm^{-1}$; however, amide III vibrations of the protein backbone of staphylococcus can be ascribed to the bands between $\tilde{\nu}=1280$ and $1225\ cm^{-1}$. The PO_2^- asymmetric stretching vibration at $\tilde{\nu}\approx1242\ cm^{-1}$ for both salmonella and staphylococcus almost overlaps with the amide III vibrations and cannot be clearly observed. However, the PO_2^- symmetric stretching vibration of salmonella can be observed at $\tilde{\nu}\approx1090\ cm^{-1}$, and PO_2^- symmetric stretches of staphylococcus appear at $\tilde{\nu}\approx1095\ cm^{-1}$ as a weak vibrational band.

In summary, with the aid of 3D nanorod supercrystals aligned vertically to the chip as a highly sensitive SERS substrate, the difference between the vibrational bands of Gram-positive and -negative bacteria can be clearly discriminated.

Layer-by-Layer-Based Vancomycin-Assembled Supercrystals as Stable Nanobiosensors to Sense Bacteria

Although the vertically aligned 3D supercrystal on a chip can efficiently amplify the weak SERS signal of bacteria, the adhesion of Gram-positive or -negative bacteria on the nanosensor needs to be improved owing to release of bacteria from the surface of the substrate after multiple washing steps. Compared with unmodified silicon chips, the adhesion capacity of salmonella on CTAB can be improved owing to electrostatic interactions between the negative charge of the cell wall of bacteria and the positive charge of the CTAB substrate. As shown in Figure S16A in the Supporting Information, a small quantity of bacteria can be retained on the CTAB-coated silicon chips after multiple washing steps; however, a number of bacteria have fallen off of the surface. However, as observed in Figure S16B in the Supporting Information, SEM results clearly indicates that the density of bacteria on the vancomycin–CTAB substrate is much higher than that on the substrate without vancomycin after multiple washing steps, which reflects that the fact that vancomycin mediation should dramatically improve trapping efficiency and increase the stability of the substrate. It can be concluded that functionalization with the antibiotic vancomycin contributes towards trapping bacteria because larger quantities of carbonyl or amine groups of the vancomycin, relative to those of CTAB, lead to strengthened binding abilities between the bacterial cell wall and vancomycin and dramatically improve the adhesion efficiency of bacteria on a chip.

Therefore, a vancomycin coating has been considered as an effective approach for increasing the adhesion capacity of bacteria on 3D nanorod supercrystals vertically aligned on a chip. As shown from the SEM image of the top view of a bacterium on the substrate in Figure 10, the bacterial cell wall is stretched to give a thin shadow attached to the substrate. This can be explained in several ways: on the one hand, surfactant-coated nanorods attached to vancomycin with the aid of interactions between amine groups of SH-PEG-NH_2 and carbonyl or hydroxyls groups of vancomycin. On the other hand, lipopolysacchar-

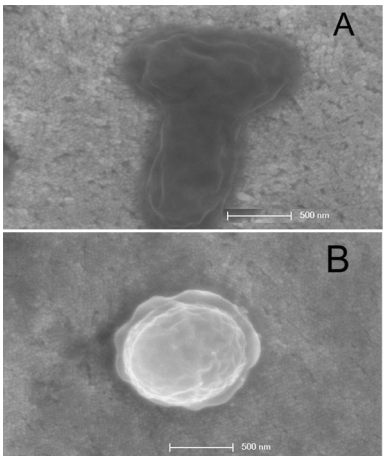

Figure 10. A) Gram-negative salmonella adhered to a substrate of vancomycin-coated 3D supercrystals vertically aligned on a chip. B) Gram-positive staphylococcus adhered to a substrate of vancomycin-coated 3D supercrystals vertically aligned on a chip.

ides of the cell wall can bind with carbonyl or hydroxyl groups of vancomycin, which lead to strong adhesion of bacteria on vancomycin-coated 3D nanorod supercrystals aligned vertically on the substrate.

As shown in Figure 11, a comparison of the SERS spectra of salmonella and staphylococcus obtained on 3D nanorod supercrystals vertically aligned on the chip with and without vancomycin indicates that the positions and envelops of vibrational bands of the bacteria are not significantly altered, which implies that introducing vancomycin does not cause interference with the SERS signal of bacteria. Moreover, the intensities of SERS of salmonella and staphylococcus from the supercrystal with a vancomycin coating are 2 and 3.5 times higher than those from the supercrystal without a vancomycin coating, respectively, which suggests that the interaction between bacteria and vancomycin-functionalized supercrystals can contribute towards increasing the SERS signal, in addition to improving the adhesion of bacteria on the supercrystal substrate. It should be noted that the greater enhancement for staphylococcus than that of salmonella reflects that the antibiotic vancomycin possesses a much stronger ability for interacting with Gram-positive bacteria than that for Gram-negative bacteria owing to differences in the cell membranes. On the other hand, a control experiment with a vancomycin-coated substrate of 3D nanorod supercrystals aligned vertically to the chip does not give a clear Raman signal, which suggests that vancomycin can give the combined advantages of efficient immobilization of bacteria and no interference with the SERS of bacteria. As shown in Figure S17 A–D in the Supporting Information, SERS comparisons of salmonella and staphylococcus on a substrate of 3D nanorod supercrystals aligned vertically to a chip, with and without vancomycin after washing treatment, indicate that a decrease in the SERS signals of salmonella or staphylococcus can be inhibited with repeated washing treatments. Hence, it can be expect that the participation of vancomycin-coated layer-by-layer assembled 3D nanorod supercrystals can act as a stable biosensor for label-free assays of microorganisms.

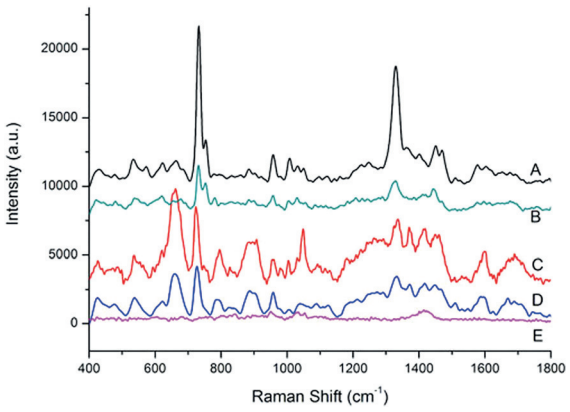

Figure 11. A) SERS spectrum of Gram-positive staphylococcus adhered to a substrate of vancomycin-coated 3D nanorod supercrystals vertically aligned on the chip. B) SERS spectrum of Gram-positive staphylococcus adhered to a substrate of 3D nanorod supercrystals vertically aligned on the chip. C) SERS spectrum of Gram-negative salmonella adhered to a substrate of vancomycin-coated 3D nanorod supercrystals vertically aligned on the chip. D) SERS spectrum of Gram-negative salmonella adhered to a substrate of 3D nanorod supercrystals vertically aligned on the chip. E) Vancomycin-coated 3D nanorod supercrystals aligned vertically on the chip.

Conclusion

Based on nanorods and nanoprisms, orientation-controlled anisometric 3D supercrystals aligned vertically and parallel to a chip could be effectively fabricated. The formation of 3D supercrystals was affected by critical factors such as the concentration of nanoparticles and surfactants, the morphology, and the components of the nanoparticles. The as-fabricated 3D nanorod supercrystals aligned vertically to the chip were successfully utilized to amplify the weak inherent SERS signal of bacteria to effectively recognize different Gram-positive and -negative bacteria without the use of labels. Moreover, to improve the stability of 3D supercrystals as bacteria biosensors, antibiotic functionalization could efficiently enhance the immobilization ability of supercrystals to avoid removal of bacteria from the nanointerface.

Experimental Section

Materials

$HAuCl_4 \cdot 4H_2O$ (99.9%), $NaBH_4$ (99%), vitamin C (99.9%), CTAB (99%), $AgNO_3$ (99.9%), SH-PEG (MW 6000), and DTNB were purchased from Sigma–Aldrich. SH-PEG-NH_2 (MW 3400) was purchased from Laysan Bio., Inc. Gram-negative salmonella (ATCC 14028) and Gram-positive staphylococcus xylosus (ZSL-3) were purchased from the China General Microbiological Culture Collection Center (CGMCC). MilliQ water, which was used throughout the experiments, was purified by using a MilliQ system.

Synthesis of AuNRs and Au@AgNRs

AuNRs could be synthesized by means of a modified seed-mediated approach.[32] First, 0.5 mM $HAuCl_4$ (10 mL) was mixed with 0.2 M CTAB (10 mL). Subsequently, 0.02 M ice-cold $NaBH_4$ (600 μL) was

added to the mixture. Vigorous stirring of the seed solution was maintained for 2 min, which settled at room temperature for 1 h. Second, 0.2 M CTAB (50 mL), 4 mM $AgNO_3$ (2.5 mL), and 1 mM $HAuCl_4$ (50 mL) were mixed to form the growth solution, followed by the addition of 0.08 M vitamin C (700 μL). Finally, the AuNRs were prepared by the addition of seed solution (120 μL) to the growth solution. The as-prepared AuNRs were centrifuged and re-dispersed in MilliQ water (10 mL). The concentration of AuNRs was about 0.5 nM, as calculated by using Beer's law and the extinction coefficients, ε, of the nanorods with an aspect ratio of about 3, which gave a concentration of $1.45\times10^9\,M^{-1}\,cm^{-1}$ according to the finite-difference time domain (FDTD) simulation.

The solution of AuNRs (2 mL) was added to a 0.1 M aqueous solution of CTAB (10 mL). A 4 mM solution of $AgNO_3$ (0.5 mL), a 0.1 M solution of vitamin C (600 μL), and a 0.1 M solution of NaOH (1.2 mL) were added to the solution. The color of the solution changed from yellow–reddish to green, which confirmed the formation of a silver shell. The as-prepared bimetallic Au@Ag core–shell nanorods were centrifuged and redispersed in MilliQ water (1 mL). According to the initial concentration of AuNRs as the core, the final concentration of Au@AgNRs could be estimated to be about 0.5 nM by assuming that silver ions were completely reduced on the surface of the AuNRs.

Synthesis of Triangular AuNPs

The AuNPs were synthesized by a modified seed-mediated approach.[27] A 10 mM solution of sodium citrate (1 mL) was diluted with freshly redistilled water (36 mL) and a 10 mM solution of $HAuCl_4$ (1 mL) was added. Subsequently, a 100 mM solution of $NaBH_4$ (1 mL) was quickly added to the mixture, which was stirred for 2 min and allowed to settle for about 3 h. For the seed-mediated growth step, three growth solutions were prepared. The first two solutions (labeled A and B) contained 10 mM $HAuCl_4$ (0.5 mL), 100 mM NaOH (0.1 mL), 100 mM vitamin C (0.1 mL), and the solution of CTAB (18 mL) purified by recrystallization. The final growth solution (designated C), contained 10 mM $HAuCl_4$ (5 mL), 100 mM NaOH (1 mL), 100 mM vitamin C (1 mL), 0.1 M KI (0.5 mL), and the as-prepared solution of CTAB (180 mL). After adding the seeding solution to solution A, the solution was quickly added to solution B, which was then quickly added to solution C. The growth solution was settled overnight and the as-prepared AuNPs were centrifuged and redispersed in MilliQ water (20 mL).

Fabricating Anisometric 3D Plasmonic Supercrystals with Controllable Orientation on a Chip

A silicon chip was first cleaned by ultrasonication in acetone, ethanol, and MilliQ water for 1 h. Then, the silicon chip was immersed in piranha solution ($H_2SO_4/H_2O_2=3:1$) at 80 °C for 1 h and rinsed with MilliQ water. The clean silicon chip was dried at room temperature.

As-prepared anisometric metallic nanoparticles (1 mL) were centrifuged at 8000 rpm for 10 min to remove the excess CTAB surfactants and redispersed in MilliQ solution (100 μL). Then, the colloidal solution of nanorods or -prisms (5 μL) was dropped onto the as-prepared silicon substrate. The samples were kept in a covered Petri dish at 25 °C with a humidity of about 80% for 24 h. Anisometric 3D supercrystals with random orientations on the chip were obtained.

A 2 $\mu g\,mL^{-1}$ solution of SH-PEG (50 or 200 μL for nanorods and -prisms, respectively) was added to freshly prepared nanorods or -prisms (1 mL) and shaken for 1 h. Then, the nanorods and -prisms were centrifuged at 10000 rpm for 5 min and redispersed in MilliQ solution (0.5 mL). A 1 nM colloidal solution of nanorods or -prisms (5 μL) was dropped onto the as-prepared silicon substrate to yield anisometric 3D supercrystals parallel to the chip at of 25 °C and a humidity of about 80% for 24 h.

A 2 $\mu g\,mL^{-1}$ solution of SH-PEG-NH_2 (50 or 200 μL for nanorods and -prisms, respectively) was added to freshly prepared nanorods or -prisms (1 mL) and shaken for 1 h. Then, the nanorods or -prisms were centrifuged at 10000 rpm for 5 min and redispersed in MilliQ solution (10 μL). A 50 nM solution of nanorods or -prisms (5 μL) containing 0.01 M NaCl was dropped onto the as-prepared silicon substrate to yield anisometric 3D supercrystals aligned vertically to a chip at 25 °C with a humidity of about 80% for 24 h.

Bacterial Cultures and SERS Sample Preparation

Powders of salmonella (ATCC 14028) and staphylococcus (ZSL-3) were dissolved in lysogeny broth (LB) nutrient (5 mL) and cultivated for 14 h in a shaker incubator at 200 rpm. By using sterile plastic inoculating loops to dip into the bacterial solution, it was placed on the LB agar base to carry out plate streaking and the plate was settled in a constant-temperature incubator and cultivated for 14 h to obtain single colonies. Single colonies were collected by using sterile plastic inoculating loops and dissolved into aquae sterilisata (1 mL). The bacterial solution (100 μL) was coated on LB agar base and incubated in a constant-temperature incubator at 37 °C. Subsequently, the bacteria were dispersed in MilliQ water and centrifuged for 10 min at 3000 rpm to protect the cell membrane. Finally, the supernatant liquid was discarded and the bacterial cells were redispersed in MilliQ water. The purified salmonella and staphylococcus bacteria were diluted to a concentration of 10^4 cfu mL^{-1}, respectively, according to the plate counting method. The density of bacterial cells could be determined by counting the number of colonies grown on a Petri dish after 12 h of cultivation.

For SERS measurements, an aqueous solution of bacteria (10 μL) was drop-casted onto a substrate of 3D Au@AgNR supercrystals aligned vertically on a chip and stored in a constant-temperature incubator at 37 °C. The sample was dried by controlled evaporation before Raman measurements were taken. Surface-enhanced Raman spectra were collected by using a 0.85 mW laser with a wavelength of $\lambda=785$ nm. Integration times were 12 s.

Characterization

TEM images were acquired with a JEM-2011 microscope operating at 200 kV. SEM images were acquired on a Quanta200FEG instrument. UV/Vis/NIR absorption spectra were recorded by using a Solidspec-3700 spectrophotometer. Surface-enhanced Raman spectra were collected by using a Renishaw Invia Reflex Raman spectrometer operating at 0.5 mW with radiation at $\lambda=785$ nm.

Acknowledgements

This work was supported by the MOST-TEKES China-Finland International Cooperation Project (grant no. 2014DFG42290) and the National Natural Science Foundation of China (grant nos. 31270770, 31400641, and 21077106).

Keywords: biosensors · crystal growth · noble metals · Raman spectroscopy · surface chemistry

[1] S. Zhao, W. Ma, L. G. Xu, X. L. Wu, H. Kuang, L. B. Wang, C. L. Xu, *Biosens. Bioelectron.* **2015**, *68*, 593.
[2] H. W. Jia, L. Qiu, J. Wang, *RSC Adv.* **2015**, *5*, 40316.
[3] V. V. Thacker, L. O. Herrmann, D. O. Sigle, T. Zhang, T. Liedl, J. J. Baumerg, U. F. Keyser, *Nat. Commun.* **2014**, *5*, 3448.
[4] L. Y. T. Chou, K. Zagorovsky, W. C. W. Chan, *Nat. Nanotechnol.* **2014**, *9*, 148.
[5] N. Liu, M. Hentschel, T. Meiss, A. P. Alivisatos, H. Giessen, *Science* **2011**, *332*, 1407.
[6] L. Rodríguez-Lorenzo, R. D. L. Rica, R. A. Alvarez-Puebla, L. M. Liz-Marzán, M. M. Stevens, *Nat. Mater.* **2012**, *11*, 604.
[7] W. Xie, B. Walkenfort, S. Schlucker, *J. Am. Chem. Soc.* **2013**, *135*, 1657.
[8] C. H. Yang, H. Y. Sui, X. W. Li, J. S. Han, X. T. Luo, H. Zhang, H. Z. Sun, H. C. Sun, Y. M. Zhou, B. Yang, *CrystEngComm* **2013**, *15*, 3490.
[9] B. D. Smith, D. J. Kirby, C. D. Keating, *Small* **2011**, *7*, 781.
[10] X. Lan, Z. Chen, G. L. Dai, X. X. Lu, W. H. Ni, Q. B. Wang, *J. Am. Chem. Soc.* **2013**, *135*, 11441.
[11] R. Y. Wang, H. L. Wang, X. C. Wu, Y. L. Ji, P. Wang, Y. Qu, T. S. Chung, *Soft Matter* **2011**, *7*, 8370.
[12] H. H. Cai, D. W. Lin, J. H. Wang, P. H. Yang, J. Y. Cai, *Sens. Actuators B* **2014**, *196*, 252.
[13] X. J. Liu, L. Zhao, H. Shen, H. X. Xu, L. H. Lu, *Talanta* **2011**, *83*, 1023.
[14] Z. N. Zhu, H. F. Meng, W. J. Liu, X. F. Liu, J. X. Gong, X. H. Qiu, L. Jiang, D. Wang, Z. Y. Tang, *Angew. Chem. Int. Ed.* **2011**, *50*, 1593; *Angew. Chem.* **2011**, *123*, 1631.
[15] B. Peng, G. Y. Li, D. H. Li, S. Dodson, Q. Zhang, J. Zhang, Y. H. Lee, H. V. Demir, X. Y. Ling, Q. H. Xiong, *ACS Nano* **2013**, *7*, 5993.
[16] C. C. Cheng, M. H. Liu, C. Y. Mou, Y. F. Chen, *RSC Adv.* **2013**, *3*, 17696.
[17] R. A. Alvarez-Puebla, A. Agarwal, P. Manna, B. P. Khanal, P. Aldeanueva-Potel, E. Carbó-Argibay, N. Pazos-Pérez, L. Vigderman, E. R. Zubazev, N. A. Kotov, L. M. Liz-Marzán, *Proc. Natl. Acad. Sci. USA* **2011**, *108*, 8157.
[18] I. S. Patel, W. R. Premasiri, D. T. Moir, L. D. Ziegler, *J. Raman Spectrosc.* **2008**, *39*, 1660.
[19] A. Sivanesan, E. Witkowska, W. Adamkiewicz, L. Dziewit, A. Kamińska, J. Waluk, *Analyst* **2014**, *139*, 1037.
[20] C. Fan, Z. Q. Hu, A. Mustapha, M. S. Lin, *Appl. Microbiol. Biotechnol.* **2011**, *92*, 1053.
[21] T. Y. Liu, K. T. Tsai, H. H. Wang, Y. Chen, Y. H. Chen, Y. C. Chao, H. H. Chang, C. H. Lin, J. K. Wang, Y. L. Wang, *Nat. Commun.* **2011**, *2*, 538.
[22] P. J. Yunker, T. Still, M. A. Lohr, A. G. Yodh, *Nature* **2011**, *476*, 308.
[23] D. H. Dahanayaka, J. X. Wang, S. Hossain, L. A. Bumm, *J. Am. Chem. Soc.* **2006**, *128*, 6052.
[24] J. E. Millstone, G. S. Metraux, C. A. Mirkin, *Adv. Funct. Mater.* **2006**, *16*, 1209.
[25] R. Jin, Y. Cao, C. A. Mirkin, K. L. Kelly, G. C. Schatz, J. G. Zheng, *Science* **2001**, *294*, 1901.
[26] M. J. Hostetler, A. C. Templeton, R. W. Murray, *Langmuir* **1999**, *15*, 3782.
[27] J. E. Millstone, S. H. Park, K. L. Shufold, L. D. Qin, G. C. Schatz, C. A. Mirkin, *J. Am. Chem. Soc.* **2005**, *127*, 5312.
[28] K. L. Kelly, E. Coronado, L. L. Zhao, G. C. Schatz, *J. Phys. Chem. B* **2003**, *107*, 668.
[29] R. Jin, Y. C. Cao, E. Hao, G. S. Mètraux, G. C. Schatz, C. A. Mirkin, *Nature* **2003**, *425*, 487.
[30] R. M. Jarvis, R. Goodacre, *Anal. Chem.* **2004**, *76*, 40.
[31] A. Lee, A. Ahmed, D. P. Dos Santos, N. Coombs, J. I. Park, R. Gordon, A. G. Brolo, E. Kumacheva, *J. Phys. Chem. C* **2012**, *116*, 5538.
[32] B. Nikoobakht, M. A. El-Sayed, *Chem. Mater.* **2003**, *15*, 1957.

Manuscript received: September 14, 2015
Accepted Article published: November 6, 2015
Final Article published: November 30, 2015